RSC Advances

ROYAL SOCIETY OF CHEMISTRY

www.rsc.org/advances

Facile-Synthesized Ultrasmall CuS Nanocrystals as Drug Nanocarries for Highly Effective Chemo-Photothermal Combination Therapy of Cancer

Xin Wang,* Qian Zhan, Li Zou, Huishang Hu, Mengxin zhang, and Jianwu Dai*

CAS Key Laboratory of Nano-Bio Interface, Suzhou Key Laboratory for Nanotheranostics, Division of Nanobiomedicine, Suzhou Institute of Nano-Tech and Nano-Bionics, Chinese Academy of Sciences, Suzhou 215123, P. R. China;

Corresponding Author: jwdai2010@sinano.ac.cn and xwang2008@sinano.ac.cn

Abstract:

Combinational chemo-photothermal therapy has been considered as a promising strategy to enhance antitumor efficiency *via* synergistic effects for cancer treatments. Here, we have developed a smart 'all-in-one' platform that conveniently combined chemo- and photothermal therapies based on ultrasmall CuS NCs, which were synthesized using a facile, low cost, and water solution reaction method. Doxorubicin (Dox)-loaded CuS drug nanocarries (CuS-Dox) were fabricated with loading capacity up to 21%. The resulting CuS-Dox exhibited pH and NIR light dual-responsiveness, demonstrating remarkably promoted Dox release under weakly acidic environment in cancer cells and enhanced intercellular uptake under an 808 nm laser irradiation. Based on in vitro cell cytotoxicity, the CuS-Dox endow an excellent chemo-photothermal synergistic effects for cancer cell death or apoptosis, attributing to both cytotoxicity of light-triggered Dox release and CuS-mediated photothermal ablation. More importantly, in vivo treatment has achieved the complete inhibition of tumor growth in 4T1-bearing mice under a low laser power density of 1.0 W/cm^2. These results demonstrate a better anti-tumor therapeutic efficacy of combined treatment in vitro and in vivo in comparison with chemotherapy or photothermal therapy alone. Our study highlights the promise of fabricating CuS-Dox drug nanocarries for highly effective chemo-photothermal combination therapy of cancer.

Key words: Chemo-Photothermal Combination Therapy, Ultrasmall CuS nanocrystals, Photothermal effect

1. Introduction

Cancer, as one of the world's most devastating diseases, has become a major public health challenge due to low effectiveness of currently available cancer treatment options.[1] To date, traditional approaches including chemotherapy and radiotherapy are widely utilized in clinical cancer therapy after surgical resection. Although important progresses have been made in antitumor therapeutic efficacy of these therapeutic approaches, they still suffer from many inevitable drawbacks: drug resistance, severe toxicity in healthy tissues, and inhomogeneous distribution of drug from the blood vessels in solid tumors with chemotherapy, incomplete resection, unavoidable tumor recurrence and low overall patient survival in surgery, and systemic side-effects as a consequence of high-dosage of X-ray irradiation and the radiation-resistance of malignant tumors with radiotherapy.[2] More recently, to overcome these drawbacks and to enhance antitumor therapeutic efficiency, the combination of therapeutic approaches with different drug and mechanism has been considered as an efficient and promising strategy to suppress tumor growth and prevent metastasis. Various combination therapies, such as gene-chemo,[3, 4] chemo-radiation,[5] and chemo-thermal,[6] have been reported as effective strategies to induce a strong synergetic effect to maximize therapeutic efficacy, overcome treatment resistance, and diminish adverse effects.[7] Among them, only chemo-radiation combinational therapy has been applied in clinical treatment, which still can incompletely meet the requirement to eradicate tumors. Therefore, there are enormous challenge to develop a combination therapy that possesses the capability to efficiently suppress tumor growth and metastases.

More recently, the combination of chemotherapy and hyperthermia has been proved to be effective in improving the sensitivity of antitumor drug around tumor and optimizing the efficacy of cancer treatment. Tremendous efforts have been devoted to the design and development of smart nanocarries-based drug delivery systems (DDSs), which are responsive to either internal (acidic pH, redox, hypoxia) or external (light, heat, magnetic field, ultrasound) stimuli, aiming to enhance intratumoral accumulation of drug, promote antitumor therapeutic efficacy, and reduce side-effects. As a noninvasive and encouraging tumor treatment modality, photothermal therapy (PTT) has attracted considerable interest in cancel therapy. It employs photothermal conversion agents (PTCAs) to strongly absorb light from near-infrared (NIR) laser (650-1100 nm) and to

convert the photon energy to local heating for cancerous cell killing or ablation. Moreover, the heat from nanoparticle-mediated hyperthermia could be located inside the tumor in an on-demand manner and the temperature elevation could be precisely tunable by controlling the time and intensity of the extrinsic light source. To date, various drug nanocarries-based DDSs have been explored to achieve the chemo-photothermal combination therapy, such as: the combination of novel metal gold (nanorods,[8] nanoshell,[9] nanocage,[10, 11] nanostars,[12] or nanotubes[13]), carbon materials (nanotubes,[14] graphene,[15] hollow nanoshpere[16]), transition metal sulfide,[17] and copper chalcogenides[18-20] based PTCAs and drug-loading mesoporous silica or organic polymer/biomolecules (gene or protein) compounds. [10, 21-26] In spite of increased drug loading capacity because of hollow mesoporous structure, these DDSs often suffer from fast release rates due to the inadequacy of effective binding sites between drug and DDSs. For those that provide sustained drug release, the drug accumulated release is not able to be precisely controlled by triggering of external stimuli. Besides, in order to obtain hollow structure, the mesoporous-based DDSs are usually prepared using complex processes, which hamper their further clinical application. Additionally, noble metal gold as PTCAs are very expensive and require severe synthesis processes. Furthermore, gold nanostructure and hollow copper sulfide as PTCAs have low photostability after laser irradiation, which leads to great weakening of photothermal conversion capability due to the disappearance of NIR absorption peak.[27] Carbon nanomaterials have also attracted much interest in PTCAs, but they show low photothermal conversion efficiency and potential long-term toxicity. Very recently, copper based NCs have been gaining interest in biomedical application, such as PTT,[19, 27-35] photoacoustic tomography (PAT),[36, 37] and DDSs,[38] owing to its low cost, low cytotoxicity, excellent electrical and optical properties, and high photothermal conversion efficiency. Most of copper chalcogenides as PTCAs have been synthesized in high-temperature organic reaction using hydrophobic oleylamine as the capping and reaction solvent.[39-41] Their hydrophobicity in nature and lack of surface functional groups hinder their further application in biomedicine. To achieve their application in biomedical fields, hydrophobic copper sulfide needs to be transferred into an aqueous phase using ligand exchange or SiO_2 coating.[20, 30, 40, 42] However, these methods involve complicated and time-consuming procedures. Moreover, the copper sulfide NCs synthesized in organic phase suffer easily from the oxidation by oxygen in air, which results in blue-color and

loss of NIR absorption properties. Therefore, to achieve the synergistic combination therapy with highly efficient antitumor efficacy by employing facile-synthesized, biocompatible and sub-10 nm nanoparticles as drug nanocarries is still a great challenge.

Previous studies revealed that the smaller-sized nanoparticles had more superior and effective tumor penetration capability, such as only 30 nm micelles could penetrate poorly permeable pancreatic tumor in comparison with other larger-size polymer micelles (50, 70, 100 nm).[43] The deep tumor-penetration is an essential prerequisite for highly effective PTT. Although the nanocarries-based DDSs could passively accumulate into the tumor site through the enhanced permeability and retention (EPR) effects, their deeper penetration into tumor tissues is significantly blocked owing to the physiological barriers of tumor.[44] It is also crucial for PTCAs as nanotherapeutic agents to be completely cleared from the human body within a reasonable period, while the sub-10 nm nanoparticles are easy to be renal clearance.[39] Thereby, ideal and smart drug nanocarries with an ultrasmall size, deep tumor-penetrating capability, and easy clearance from body is in great desire for chemo-photothermal combination therapy of cancer.

Motivated by the above requirements, we developed the pH and NIR light dual-responsive CuS-Dox drug nanocarries based on ultrasmall CuS NCs for highly effective chemo-photothermal combination therapy of breast cancer. A facile, low cost, and water solution based method was employed to synthesize ultrasmall and water soluble poly (acrylic acid) (PAA)-conjugated CuS (PAA-CuS) NCs, which exhibit high photothermal conversion efficiency and excellent biocompatibility. Layer-by-layer (LBL) self-assembly was applied to fabricate the smart CuS-Dox drug nanocarries on a large scale based on strong electrostatic interaction between negatively charged PAA with positively charged Dox and poly(allylaminehydrochloride) (PAH), as shown in Scheme 1. High loading capacity up to 21% was achieved in this drug deliver nanoplatform. The PAH coating provides a protective layer to improve the stability and biocompatiblility of CuS-Dox. The CuS-PAA-Dox-PAH (abbreviated as CuS-Dox) drug nanocarries were engineered as pH and NIR light dual-responsive DDSs, in which the intracellular uptake and release of Dox payload could be triggered by the hyperthermia effect. More importantly, the tumor growth in 4T1-bearing mice model has been completely suppressed with the enhanced chemotherapeutic efficiency and localized hyperthermia at a low laser output power density of 1.0 W/cm^2. Our work highlights the facile fabrication of the DDSs

nanoplatform based on the ultrasmall CuS NCs to achieve highly effective chemo-photothermal combination therapy of cancer.

2. Experimental Section

2.1 Materials and Measurement: All chemicals and reagents were of analytical grade and used directly without further purification. Cupric chloride ($CuCl_2$), sodium hydroxide (NaOH), hydrazine anhydrous (N_2H_4:H_2O), disodium sulfide (Na_2S), Dimethyl sulfoxide (DMSO) and anhydrous ethanol were purchased from the Sinopharm Chemicals Reagent Co. (Shanghai, China). Poly (acrylic acid) (PAA, MW = 1800), poly (allylamine hydrochloride) (PAH, MW=15 000), calcein acetoxymethyl ester (calcein-AM), propidium iodide (PI), and 3-[4,5-Dimethylthiazol-2-yl] -2,5-diphenyltetrazolium bromide (MTT) were purchased from Sigma-Aldrich. Doxorubicin (Dox, 99%) was obtained from Shanghai Sangon Biotech Co. Ltd. Fetal bovine serum (FBS), RPMI-1640 cell culture medium, and Penicillin-streptomycin solution were supplied by Gibco Life Technologies. Deionized water with resistivity of 18.2 MΩ was obtained from a Milli-Q Biocel water purification system. Transmission electron microscopy (TEM) photographs were recorded on a FEI Tecnai G2-F20 U-TWIN (200 kV) transmission electron microscope. Energy dispersive X-ray spectroscopy (EDS) (FEI Quanta400FEG) was used to determine the chemical composition of the products. Powder X-ray diffraction (XRD) data were measured on a D8 Advance Bruker X-ray diffractometer with Cu-Kα radiation (I = 1.5418 Å). X-ray photoelectron spectroscopy (XPS, Lb250) was used to examine the electron binding energy of the products. The UV-vis absorption spectra were recorded using a Perkin Elmer Lambda-25 UV-vis spectrophotometer. Fourier-transform infrared (FTIR) spectra were measured with a Thermo Nicolet 6700 spectrometer. Fluorescence spectra were acquired by a Hitachi F-4600 fluorescence spectrophotometer. DLS and Zeta potential measurements were performed on a Zeta sizer Nano ZS instrument (Malvern Instruments, U.K.) with a 633 nm He-Ne laser. A continuous wave fiber-coupled diode laser system (808 nm, 5 w) was purchased from Changchun Femtosecond Tech Co. The thermographs were performed using a FLIR A325sc LWIR thermal imaging Camera. The concentration of Cu in sample was measured by inductively coupled plasma atomic emission spectroscopy (ICP-AES). Intracellular fluorescence imaging

was monitored by fluorescence microscopy using a Nikon Ti-Eclipse microscope.

2.2 Preparation of PAA-CuS NCs. In a typical synthesis, $CuCl_2$ (0.05 mmol) was dissolved in 25 mL deionized water containing 14.4 mg of PAA, followed by the addition of a 25 mL of NaOH solution (pH 9.0). After being stirred for 10 min, 6.4 μL of hydrazine anhydrous was added into the above mixture slowly and stirred for another 10 min. Then, a 200 μL aqueous stock solution of disodium sulfide (Na_2S, 320 mg/mL) was added and heated at 60 ℃ for 2 h until a dark-green solution was obtained. After the reaction, the resultant mixture was collected by centrifugation and washed with deionized water and anhydrous ethanol for three cycles to remove the unreacted ions. The PAA-conjugated CuS NCs were obtained and stored at 4 ℃.

2.3 Photothermal Effect Measurements. An aqueous suspension (2 mL) containing CuS NCs at a series of different concentrations was introduced into a quartz cuvette and exposed to 808 nm laser with tunable output power density for 10 min. The temperature variation was monitored using a digital thermometer with thermocouple probe.

2.4 Drug Loading. The CuS-Dox nanocarries were fabricated via polyelectrolyte LBL self-assembly method. Briefly, 5 mL PAA-CuS nanocystals dispersed an aqueous solution (96 μg/mL) was mixed with 60 μL of 5 mg/mL free Dox, and then were stirred for 24 h at room temperature. The positively charged Dox was bound onto the surface of the negatively charged PAA-CuS nanocystals through electrostatic interaction. The dispersion was centrifuged by using Millipore Centrifugal Filter Concentrator (NMWL: 3,000) to collect the CuS-PAA-Dox nanoparticles. The Dox concentration in the suspension was obtained by UV-vis absorption spectra at 490 nm to calculate the Dox loading capacity. Afterward, the purified CuS-PAA-Dox was added by 2 mL of oppositely charged PAH (5.0 mg/mL) in 0.5 M NaCl solution and the mixture solution was stirred for 24 h at room temperature. The unconjugated PAH was then removed by the centrifugation at 10,000 rpm for 10 min and repeatedly washed with PBS. The resulting CuS-Dox was redispersed in PBS buffer solution and stored at 4 ℃. Loading capacity and encapsulation efficiency of Dox were calculated by the following equations: Loading capacity = (initial weight of Dox – weight of unbounded Dox) / (weight of CuS-Dox); Encapsulation Efficiency = (initial weight of Dox – weight of unbounded Dox) / (initial weight of Dox). Dox encapsulation efficiency was 47% and loading capacity reached up to 21%.

2.5 In Vitro pH and NIR Light Dual-Responsive Release Study. To investigate acidic

pH-responsive drug release, 5.0 mL of CuS-Dox solution sealed in a dialysis bag (MWCO = 3500) was submerged in 50 mL of different pH buffers (5.0 and 7.4) and stirred at 37 ℃ for 36 h. At predetermined time interval, 3.0 mL of outside buffer solution was collected and measured by UV-vis spectrometer to determine the amount of released Dox according to the typical absorption at 490 nm, and then returned to the original solution. The NIR light-triggered release properties of CuS-Dox in PBS buffer (pH 5.0) were evaluated under repeated irradiation of 808 nm laser at different power densities over a period of 10 min, followed by 60 min interval with the turned-off laser. At desired time intervals, the same procedures described above were performed to quantify the amount of released Dox through NIR light triggering.

2.6 Cell Line and Animals. Parental MCF-7 human breast cancer cell line and 4T1 murine breast cancer cell line were supplied by American Type Culture Collection (ATCC). Both kinds of cells were cultured in RPMI 1640 cell culture medium containing 10% fetal bovine serum, 100U mL^{-1} of penicillin G sodium and 100 mg mL^{-1} of streptomycin sulfate. Cells were maintained at 37 ℃ in an incubator with a humidified atmosphere and 5% CO_2 concentration. Female BALB/c mice (18-22 g) were obtained from Shanghai SLAC Laboratory Animal Co., and acclimatized under the animal care facility for 5 days prior to the animal experiments, which was performed under protocols approved by the Institutional Animal Care and Use Committee (IACUC).

2.7 In Vitro Photothermal Ablation of Cancer Cells. To examine the photothermal ablation of cancer cells in vitro, MCF-7 cells (1×10^4 cells per well) were seeded in 48-well plates and incubated overnight at 37 ℃ in a humidified 5% CO_2 atmosphere. After being rinsed with PBS, the cells were incubated CuS NCs with three different concentrations of 50, 80, 100 μg/mL for 4 h at 37 ℃ under same condition. After that, the cells of experiment group were rinsed again with PBS and immersed in 50 μL of fresh culture medium, and subsequently irradiated under 808 nm light with output power density of 1.0 W/cm^2 for 10 min. After another 4 h incubation, cells were stained with calcein-AM and PI for separate visualization of live cells and dead/late apoptotic cells according to the manufacturer's advised protocol. After rinsing with PBS, the cells were fixed with 5% polyoxymethylene. An inverted fluorescence microscopy was applied to observe a green fluorescence color caused by calcein-AM indicating live cells and a red fluorescence color caused by PI indicating dead cells.

2.8 Cellular Uptake and in Vitro Cytotoxicities of CuS-Dox Nanocarries. The fluorescence of

Dox was monitored to study intercellular uptake of CuS-Dox in MCF-7 cells by using fluorescence microscopy. In brief, MCF-7 cells were seeded on the circle coverslips in a 24-well plate at the density of 2×10^4 cells per well in 0.5 mL medium and incubated at 37 ℃ overnight prior to the experiment. Then, the cells were cultured in medium containing 5 μM free Dox or equivalent dose of CuS-Dox. After 2 h incubator at 37 ℃, the cells incubated with CuS-Dox were treated with or without 808 nm laser irradiation at a power density of 1.0 W/cm^2 for 6 min, and then incubated for additional 2 h. Afterward, the cells were removed of medium, rinsed three times with PBS, fixed in 5% of polyoxymethylene solution and then imaged by fluorescence microscopy.

The cytotoxicities of free Dox, CuS and CuS-Dox on 4T1 and MCF-7 cells were separately evaluated by the MTT assay. Briefly, cells were seed in 96-well plates at a density of 8×10^3 per well for 24-h assays and allowed to culture at 37 ℃ overnight. The culture medium was replaced and the cells were incubated with fresh medium containing free Dox, CuS and CuS-Dox. The groups of free Dox and CuS-Dox have the same concentration of Dox. After incubating for 24 h, the cells were removed of the Dox-containing medium and cultured in 100 μL fresh medium containing MTT (1 mg/mL) at 37 ℃ for 4 h. Afterward, the cell medium containing MTT was replaced with 150 μL DMSO. After shaking the 96-well plates at room temperature for 15 min, the absorbance of each well at 570 nm was examined by a micro-reader (Bio-Rad Model 680) to determine the relative cell viabilities.

2.9 In Vitro Chemo-Photothermal Combination Therapy. To investigate the synergistic therapeutic effect of CuS-Dox on breast cancer MCF-7 cells, the cell viabilities after various treatments were evaluated by standard MTT assay. In brief, cells were seeded in the 96-well plate at a density of 8×10^3 per well and incubated at 37 ℃ for 12 h. The culture medium was changed and cells were incubated with complete culture medium containing free Dox, CuS NCs and CuS-Dox. The groups of free Dox and CuS-Dox have the same Dox concentration. While the groups of CuS and CuS-Dox have an equivalent CuS concentration. After 4 h incubation, cells were rinsed three times with PBS and then were added with fresh complete medium. The cells of the groups, free Dox, CuS, and CuS-Dox, were exposed to 808 nm light at output power density of 1.0 W/cm^2 for 6 min and then incubated at 37 ℃ for another 24 h. Finally, the relative cell viabilities were determined by standard MTT assay according to the same procedure

as mentioned above.

2.10 In Vivo Chemo-Photothermal Combination Therapy. 4T1 murine breast cancer cells were cultured under standard protocol. 4T1 tumors were generated by subcutaneous injection of 1 × 10^6 cells suspended in PBS (100 μL) into the back of female BALB/c mice. When the tumors volume reached about 100 mm^3, mice were anesthetized, randomly divided into five groups (n = 3), and intratumorally injected with 50 μL of PBS, free Dox, CuS, and CuS-Dox at an equivalent Dox or CuS dose of 2.0 or 10 mg/kg, respectively. Two hours after injection, the tumors were locally irradiated by 808 nm laser at an output power density of 1.0 W/cm^2 for 10 min. Temperature elevation in tumor region under laser irradiation was recorded with an IR thermal imaging camera. The tumor proliferation rates were monitored every day with a digital caliper and the body weights were determined using an electronic balance, respectively. The tumor volume was calculated according to the equation: Volume = (tumor length) × $(\text{tumor width})^2/2$. All mice were sacrificed on Day 12, and the excised tumors were photographed. For histological examination, the tumors were fixed in 10% neutral buffered formalin, processed routinely into paraffin, sectioned at 5 μm thicknesses, stained with hematoxylin and eosin (H&E) and examined by a digital microscope.

3. Results and Discussion

3.1. Preparation and Characterization of PAA-CuS NCs

PAA-CuS NCs were synthesized in aqueous solution by reacting $CuCl_2$ and Na_2S in the presence of poly (acrylic acid) (PAA) at 60 ℃ for 2 h. PAA with abundant carboxyl ($-COO^-$) groups was utilized to stabilize the CuS NCs by providing the fine stability and water solubility due to strong conjugation of Cu ions with carboxyl groups from PAA and the highly negative Zeta potential of -24 mV. It is worthwhile to note that the PAA acts not only as the capping agent for stabilizing CuS NCs, but also as the template for homogeneous growth of CuS NCs to obtain uniform distribution of particle size. Representative transmission electron microscope (TEM) images (Figure 1a) show that the as-synthesized PAA-CuS NCs display good dispersity. From the magnified TEM image shown in Figure1b, the CuS NCs have a well-defined spherical morphology with a uniform size distribution and an average diameter of 3.5 nm. Moreover, the HRTEM image (the inset of Figure 2b) displays that the lattice spacing (d-spacing) of a (102)

plane is about 0.3 nm. The crystal structures of CuS NCs were examined by power X-ray diffraction (XRD). The XRD patterns of the CuS NCs (Figure S1a in supporting information) are indexed as covellite-phase CuS (JCPDS file number 79-2321). The diffraction peaks were distinctly broadened, indicating the small size of the CuS NCs. No obvious impurity peaks were observed, suggesting a high quality of the synthesized CuS NCs. Furthermore, the elemental compositions and chemical speciation of the sample was determined by energy dispersive X-ray spectra (EDS), which revealed 1:1 molar ratio of Cu and S (Figure S1a in supporting information). The XPS spectra in Figure S1c,d (in supporting information) display the binding energies of Cu 2p3/2, Cu 2p1/2 and S 2p peaks about 935, 953, and 163 eV, respectively, which further confirm the elemental composites and surface electronic state of the obtained CuS NCs and is in good agreement with the above XRD and EDS results.

3.2. Optical Properties and Photothermal Effect of CuS NCs

The most impressive feature of CuS NCs is surface plasmon resonance that exhibits broad and very strong peaks in the NIR region. The UV-vis absorbance spectrum (Figure 2a) of the PAA-CuS NCs dispersed in water exhibits a short-wavelength absorption edge at approximately 580 nm and an increased absorption with the increase of wavelength in the NIR region (λ=600-1100 nm). The strong NIR absorption is mainly attributed to localized surface plasmon resonance of high-concentration free carrier (holes) due to many Cu deficiencies in the CuS NCs. Importantly, such a strong absorption of CuS NCs in the NIR region inspires their potential application as promising PTCAs for NIR laser photothermal ablation of cancer cells.

To evaluate the photothermal effect, the temperature elevation of aqueous dispersion containing CuS NCs at different concentration was examined upon irradiation of an 808 nm laser at power density of 2.3 W/cm^2 for 10 min. After 10 min laser irradiation, Figure 1d shows that the temperature elevation of the aqueous dispersion containing CuS NCs increased by 16-44 ℃ from room temperature with an increase of the CuS concentration from 6 to 96 μg/mL, which was also visualized in corresponding images taken by an infrared thermal camera (Figure 1e). In contrast, the temperature elevation of water in the control experiment was less than 7 ℃. Figure 1f plots the temperature elevation with regard to CuS concentration, in which the temperature increase curve grows rapidly with increasing CuS concentration. This is owing to the logarithmic

absorbance dependence on the fraction of incident radiation. Furthermore, an obvious dependence of temperature elevation on laser power density was observed when the CuS concentration was fixed at 96 μg/mL (Figure 1g). When the incident laser output density as low as 0.68 W/cm^{-2}, a temperature elevation of 15 ℃ can be obtained, which is well beyond the required temperature for killing cancer cells. It is worthwhile to note that after the CuS NCs solution was exposed to laser over an hour, no variation in the absorbance spectrum of CuS NCs was observed, which indicates good photostability of the synthesized CuS NCs.

To investigate the photothermal conversion efficiency of CuS NCs aqueous solution, a method reported by Roper *et al* was used for calculation.[45] After the solution (24 μg/mL) reached a steady state temperature under irradiation of 808 nm laser, the temperature decrease of the solution was recorded as a function of time without light source to determine the rate of heat transfer from the solution to the environment (Figure 1h). Following the procedure reported by Roper *et al* and the fitted results of the measured cooling curve (Figure 1i), the photothermal conversion efficiency of the CuS NCs was calculated to be 19.5% (detailed in the supporting information). This value is close to that of gold nanorods (21%)[20] but lower than that of recently reported $Cu_{7.2}S_4$ NCs, due to the bigger size of $Cu_{7.2}S_4$ NCs (more than 10 nm) and thus larger absorption cross section.[41]

3.3. Fabrication and Triggered Release of CuS-Dox Drug Nanocarries

In our study, the pH and NIR light dual-responsive CuS-Dox drug nanocrarries were easily synthesized via ployelectrolyte LBL electrostatic self-assembly. Polyelectrolytes such as PAA and PAH are widely used to fabricate pH-responsive antitumor drug release systems.[46, 47] Firstly, Dox was encapsulated on the surface of the negatively charged PAA-CuS NCs, as shown in Scheme 1. Based on the previous reports, the pKas of Dox and PAA are 8.6 and 4.8, respectively.[48] Hence, a strong electrostatic interaction occurred between positively charged Dox and negatively charged PAA on the surface of CuS NCs when Dox was added into the dispersion solution of PAA-CuS NCs. Subsequently, the negatively charged PAA on the surface CuS NCs were further modified by the cationic polymer PAH with a molecular weight of 15 kDs by electrostatic interaction, resulting in a PAH coating for CuS-PAA-Dox nanoparticles. Zeta

potential measurement was performed to monitor the LBL self-assembly of polyelectrolyte (PAA and PAH). Zeta potential of -24 mV for PAA-CuS NCs was changed to be +26 mV for CuS-Dox. The hydrodynamic diameter of the resulting CuS-Dox nanoparticles, determined by dynamic light scattering (DLS) (Figure 1c), was increased after LBL self-assembly process. The CuS-Dox products have good dispersibility with an average hydrodynamic diameter of about 7.1 nm and keep stable even after half a year for storage. Comparing to the initial Dox and PAA-CuS NCs, the UV-vis-NIR absorbance spectrum of the CuS-Dox possesses both strong characteristic absorption peak of Dox and broad plasma absorption band of the CuS NCs at the NIR region, which verifies successful loading of Dox onto the CuS NCs (Figure 2a). The Dox loading resulted in a significant change of the color of the CuS NCs solution from dark-green to pink, which was easily distinguishable to the naked eye (Inset of Figure 2a). The formation of CuS-Dox was further characterized by FTIR, as shown in Figure S2. The FTIR spectra of free Dox, CuS-PAA, and CuS-Dox show the characteristic absorption peaks of Dox (1718 and 1615 cm^{-1}) and PAA (1612 and 1513 cm^{-1}), respectively. Figure 2b depicts that continued increase in the Dox concentration over 3 mg/mL quenched the fluorescence of Dox in the CuS-Dox solution due to the aggregation of Dox and strong interaction between Dox and CuS NCs, suggesting successful loading of Dox on the CuS NCs. Furthermore, the drug loading capacity and encapsulation efficiency of Dox in the CuS NCs were calculated about 21% and 47%, respectively, demonstrating that Dox was efficiently loaded on the surface of ultrasmall CuS NCs.

To examine the pH-responsiveness of the CuS-Dox, the Dox release profiles under different environmental pH values were investigated. The release amount of Dox at 37 ℃ through a dialysis membrane, which allows for penetration of free Dox molecules but not the CuS-Dox nanocarries into the surrounding solution bath, was determined by the absorbance peak intensity at about 490 nm of the supernatant. At pH 7.4, the release amount of Dox was only 13% over the course of 36 h, suggesting the high stability of CuS-Dox at neutral condition (Figure 2c). In contrast, approximately 80% of Dox was released from CuS-Dox at pH 5.0 over 36 h. Additionally, the release profile for pH 5.0 solution shows sustained release over a long period (> 36 h) as compared with that of free Dox molecules, which completely release within 10 h. The release percentages in pH 5.0 solution were 63, 70, and 78% after 12, 24, and 36 h, respectively.

The abundant carboxyl groups in PAA molecules were protonated at low pH (~ 4.5-6.0) to weaken the electrostatic interaction between PAA and Dox. The pH-responsiveness is particularly advantageous for cancer treatment and minimizes extracellular loss of drug molecules before reaching tumor targets as well as potential damage to normal cells, thus enhancing the antitumor therapy. To test the NIR light-responsiveness of CuS-Dox, the release profile of Dox was also measured in the pH 5.0 PBS buffer solution with and without NIR laser irradiation (808 nm) for 10 min and 60 min, respectively. Figure 2d displays that when the CuS-Dox was irradiated for 6 ×10 min at the output power density of 0.66 W/cm^2, the Dox release was sharply increased to 50%, higher than that of Dox released from the control (25%). Furthermore, a power-dependent release of Dox was observed from the CuS-Dox and over 80% of Dox was released within 6 h at the power of 1.83 W/cm^2. The results revealed that a control release of Dox from CuS-Dox could be achieved by NIR light-stimuli local hyperthermia. The remarkable spatial/temporal resolution profiles imply a good potential of CuS-Dox as on-demand drug delivery system to enhance antitumor therapy efficacy.

3.4. Cell Internalization and Cytotoxicity of CuS-Dox

To investigate the internalization of CuS-Dox, cellular uptake of Dox under irradiation of an 808 nm laser was evaluated by fluorescence microscopy. As shown in Figure 3a and 3b, higher fluorescence intensity was found in MCF-7 cells treated with CuS-Dox than those with free Dox, indicating higher intracellular uptake efficacy of CuS-Dox compared to free Dox. Additionally, the Dox fluorescence inside cells incubated with CuS-Dox was further enhanced after laser irradiation compared to those without irradiation, clearly suggesting that more free Dox molecules were released from the intracellular CuS-Dox (Figure 3c). This result shows that the mild phototherml heating by the 808 nm laser can increase the cell membrane permeability to enhance the cell internalization of CuS-Dox and improve the intercellular delivery of Dox for highly effective antitumor therapy. Therefore, the CuS-Dox can play a remarkable role in regulating the cell internalization of Dox molecules and enhance their intracellular accumulation under NIR light irradiation.

Next, we evaluated the cytotoxicity of CuS-Dox in both 4T1 and MCF-7 cells using standard MTT assay (see the methods in experiment section). 4T1 and MCF-7 cells were

incubated in culture medium containing CuS NCs, free Dox, and CuS-Dox for 24 h at different Dox concentrations. As shown in Figure S3 (in supporting information), the CuS-Dox displayed a significant cytotoxicity against 4T1 and MCF-7 cells with IC_{50} (half-inhibitory concentration) of 2.78 and 3.05 μM, respectively. Furthermore, the CuS-Dox demonstrated higher cytotoxicity to cancer cells than free Dox at the same concentration, indicating that Dox was more effectively transported into the cells by CuS-Dox than free Dox. The raw CuS NCs showed negligible toxicities within all the tested concentrations (cell viability > 90%). As a result, the CuS-Dox can serve as excellent carrier candidates for drug delivery and disease therapy.

3.5. In Vitro Chemo-Photothermal Combination Therapy

Inspired by the outstanding photothermal conversion properties, we irradiated MCF-7 cells treated with the ultrasmall CuS NCs with an 808 nm NIR laser to evaluate the photothermal ablation of cells. After variable treatments with CuS NCs and laser, the cell viability was measured by staining cells with Calcine AM and PI to differentiate live (green) and dead (red) cells, respectively, and then imaged by a fluorescence microscope. Cells treated with PBS solution were used as control. As shown in Figure 4a, MCF-7 cells treated with CuS NCs plus a NIR laser experienced substantial cellular death, indicating that CuS NCs mediated effective photothermal ablation of MCF-7 cancer cells. The cell death rate increased with the increase of CuS concentration under irradiation of the same power density and time. In contrast, no apparent change in cell viability and density was observed when cells were treated with CuS NCs (100 μg/mL) alone or the NIR laser alone compared with the negative control without the NIR laser and CuS NCs (Figure 4b). These results suggest that the CuS NCs can effectively kill cancer cells through the photothermal effect induced by NIR irradiation.

To further investigate the effect of chemotherapy, photothermal therapy and their combination therapy in vitro, the relative cell viabilities of MCF-7 cells treated with CuS NCs, free Dox, and CuS-Dox with or without NIR irradiation were evaluated by using the MTT assay. Herein, the CuS-Dox and CuS-Dox+Laser groups have an equivalent Dox dosage to free Dox group. The cell viabilities (Figure 4c) and the inhibition rates (Figure 4d) were measured as a function of the CuS concentration. These groups show decreased cell viability with the increase of concentration. The CuS+Laser group (Figure 4d, red curve) exhibits increasing cell death with

increasing the concentration, consistent with the results of Figure 4a. The Dox released from the CuS-Dox nanocarries shows higher therapy capability than free Dox and the cytotoxicity exhibits in a dose-dependent manner (Figure 4d, pink and green curves), which demonstrates the CuS NCs can serve as drug nanocarries to enhance chemotherapy. More importantly, the CuS-Dox+Laser group (Figure 4d, red curve) shows a remarkably enhanced inhibition effect comparing with that of the free Dox, CuS+Laser, and CuS-Dox without laser at equivalent concentrations. Fox example, when MCF-7 cells were treated with CuS-Dox+Laser (CuS concentration = 40 μg/mL), the cell viability was remarkably reduced to 8%, which is clearly lower than that of the CuS+Laser and the CuS-Dox without laser, suggesting enhanced antitumor activities of CuS-Dox when irradiated with an 808 nm laser. Therefore, the CuS-Dox showed significantly higher cell-killing ability than the separate photothermal therapeutic efficacy of CuS NCs and chemotherapeutic efficacy of free Dox at the equivalent CuS dosage or Dox concentration, indicating the synergistic effect of chemo-photothermal therapy. The developed CuS-Dox drug nanocarries not only possess the photothermal ablation of cancer cells but also act as drug delivery vehicles for chemotherapy of cancer, and importantly the combination of chemotherapy and photothermal effect demonstrates higher antitumor therapeutic efficacy. All these results indicate that the combination of chemotherapy and photothermal therapy through the fabrication of CuS-Dox as drug carries would be expected to remarkably enhance antitumor therapeutic efficacy and become a promising approach for cancer therapy.

3.6. In Vivo Chemo-Photothermal Combination Therapy

Inspired by in vitro synergistic performance of chemo-photothermal combination therapy of cancer cells, an infrared thermal camera was used to record the temperature change in the tumor region under an 808 nm laser irradiation. 4T1 tumor-bearing BALB/c mice were intratumorally injected with PBS, free Dox, CuS, and CuS-Dox for 2 h, then anesthetized. As shown in Figure S4, the IR thermal graphic images show that the tumor surface temperatures of mice injected with CuS or CuS-Dox rapidly increased to about 48 ℃ in 3 min and maintained for 10 min under laser irradiation (1.0 W/cm^2). The elevation of tumor temperature mainly attributes to the superior heat-generating ability of CuS NCs. Moreover, the maximal temperature of tumor in CuS+Laser or CuS-Dox+Laser treated group is far beyond threshold required to induce thermal

ablation of cancer cells. In contrast, only slight increase in temperature (~2 ℃) was observed from the mice treated with free Dox+Laser after 10 min irradiation. Although a slight temperature increase was observed in the Dox+Laser groups, the temperature in the tumor region was not enough high to kill the cancer cells effectively. Additionally, no variation in surface temperature was observed on the groups treated with PBS+Laser and CuS-Dox alone (without laser irradiation). These results clearly prove the great potential of CuS NCs for PTT.

The comparable studies of effectiveness in inhibiting tumor were further performed to investigate in vivo therapeutic efficiency of the CuS-Dox. 4T1 tumor-bearing mice were divided five groups randomly (n=3), which were treated with PBS+Laser, free Dox+Laser, CuS+Laser, CuS-Dox+Laser, and CuS-Dox without laser, respectively. The area of tumor upon irradiation became whitish immediately due to disruption of blood perfusion and further became black scars on the original tumor sites after 1-day treatment. The representative images of tumor-bearing mice from each group are shown in Figure 5. Tumor areas were clearly observable in PBS+Laser, free Dox+Laser, CuS+Laser, and CuS-Dox without laser, but were almost eliminated with necrotic scar left at the original tumor site of the CuS-Dox+Laser group after 9-day treatment. Additionally, the mice were observed daily for clinical symptoms and the tumor size were measured using a caliper every day after laser treatment. There was a statistically significant difference in tumor growth rates between the treatment groups over times. As shown in Figure 6a, the tumor growth profiles show that the tumor size of CuS-Dox+Laser group shrank gradually to zero within 12 days after laser irradiation. On the contrary, the average tumor sizes of the PBS+Laser (as control group), free Dox+Laser, CuS+Laser, and CuS-Dox without laser treated mice were approximately13-, 10-, 6.4-, and 3.7-folds larger than the initial size after about 12 days of feeding, respectively. The CuS-Dox without laser exhibited a higher tumor inhibitory rate than free Dox owing to more readily cell internalization of CuS-Dox than free Dox. Besides, due to high toxicity usually leading to a significant weight loss, the body weight of the mice for all groups were measured during the treatments and no significant weight loss was observed for all groups (Figure 6b). This indicates the CuS-Dox+Laser treatment has very low toxicity. On the 12th day, mice were sacrificed and tumors were excised. The tumor photograph of each group after the treatment is shown in Figure 6c, which confirmed the CuS-Dox+Laser treated group significantly higher tumor growth inhibition than free Dox+Laser, CuS+Laser, and CuS-Dox

without laser treated groups. To further confirm the antitumor therapeutic efficacy, a histological analysis of resected tumors was performed after 12-day treatment. From the hematoxylin-eosin (H&E) stained images shown in Figure 6d, tumors of mice treated with CuS-Dox+Laser showed large area of apoptosis and necrosis with vacuoles and membrane destruction, while mice receiving treatment of PBS+Laser, free Dox+Laser, CuS+Laser, and CuS-Dox without laser had tumor with large regions of viable cancer cells and massive vasculature structures. Under laser irradiation, the CuS-Dox could remarkably enhance antitumor therapeutic efficacy in vivo than individual treatment (Dox+Laser or CuS+Laser), which was probably attributed to (1) control release of Dox from the CuS-Dox nanocarries, (2) deep penetration of ultrasmall CuS-Dox in tumor, and (3) synergistic effect of chemo-photothermal combination therapy. Therefore, these results revealed the CuS-Dox could be a powerful agent for chemo-photothermal combination therapy of cancer in vivo.

4. Conclusion

In summary, a novel ultrasmall CuS NCs-based nanotherapeutic agent, which combines two different treatment modalities, chemotherapy and PDT, into one single nanoplatform, has been developed for highly effective antitumor therapeutic efficacy of breast cancers in vivo. The ultrasmall and water soluble CuS NCs were synthesized using a facile and water solution reaction method and demonstrated strong NIR region absorption, high photothermal conversion efficiency, and excellent biocompatibility in vitro. Moreover, the pH and NIR light dual-responsive CuS-Dox drug nanocarries that were fabricated by LBL electrostatic self-assembly can simultaneously enhance the release and deep tumor penetration of Dox payload when combined with photothermal therapy under NIR laser irradiation, thus significantly improving the antitumor therapeutic efficacy both in vitro and in vivo. Therefore, the CuS-Dox drug nanocarries are a promising nanoplatform to achieve synergistic effects of chemo-photothermal combination therapy of cancers.

Supporting Information: XRD, EDS, XPS, FTIR, Cell Viability, and IR Thermo Images.

Acknowledgements

The work was supported financially by the National Natural Science Foundation of China (Grant Nos. 11174324 and 10804082) and by the Youth Innovation Promotion Association of Chinese Academy of Sciences (Grant Nos. 2011235).

References

1. G. Yang, J. Wang, Y. Wang, L. Li, X. Guo and S. B. Zhou, *Acs Nano*, 2015, **9**, 1161-1174.
2. S. Wang, X. Li, Y. Chen, X. Cai, H. Yao, W. Gao, Y. Zheng, X. An, J. Shi and H. Chen, *Adv. Mater*, 2015, **27**, 2775-2782.
3. S. Liu, Y. Guo, R. Huang, J. Li, S. Huang, Y. Kuang, L. Han and C. Jiang, *Biomaterials*, 2012, **33**, 4907-4916.
4. D. Cheng, N. Cao, J. Chen, X. Yu and X. Shuai, *Biomaterials*, 2012, **33**, 1170-1179.
5. C. N. Chu, P. C. Chen, L. Y. Bai, C. H. Muo, F. C. Sung and S. W. Chen, *Clin. Otolaryngol.*, 2013, **38**, 39-47.
6. Z. Zhang, J. Wang and C. Chen, *Adv. Mater.*, 2013, **25**, 3869-3880.
7. L. Miao, S. Guo, J. Zhang, W. Y. Kim and L. Huang, *Adv. Funct. Mater.*, 2014, **24**, 6601-6611.
8. D. Wang, Z. Xu, H. Yu, X. Chen, B. Feng, Z. Cui, B. Lin, Q. Yin, Z. Zhang, C. Chen, J. Wang, W. Zhang and Y. Li, *Biomaterials*, 2014, **35**, 8374-8384.
9. J. Yang, J. Lee, J. Kang, S. J. Oh, H.-J. Ko, J.-H. Son, K. Lee, J.-S. Suh, Y.-M. Huh and S. Haam, *Adv. Mater.*, 2009, **21**, 4339-4342.
10. Z. Wang, Z. Chen, Z. Liu, P. Shi, K. Dong, E. Ju, J. Ren and X. Qu, *Biomaterials*, 2014, **35**, 9678-9688.
11. T. Sun, Y. Wang, Y. Wang, J. Xu, X. Zhao, S. Vangveravong, R. H. Mach and Y. Xia, *Adv. Healthcare. Mater.*, 2014, **3**, 1283-1291.
12. H. Chen, X. Zhang, S. Dai, Y. Ma, S. Cui, S. Achilefu and Y. Gu, *Theranostics*, 2013, **3**, 633-649.
13. S. Ye, G. Marston, J. R. McLaughlan, D. O. Sigle, N. Ingram, S. Freear, J. J. Baumberg, R. J. Bushby, A. F. Markham, K. Critchley, P. L. Coletta and S. D. Evans, *Adv. Funct. Mater.*, 2015, **25**, 2117-2127.
14. J. Liu, C. Wang, X. Wang, X. Wang, L. Cheng, Y. Li and Z. Liu, *Adv. Funct. Mater.s*, 2015, **25**, 384-392.
15. L. Feng, K. Li, X. Shi, M. Gao, J. Liu and Z. Liu, *Adv. Healthcare. Mater.*, 2014, **3**, 1261-1271.
16. L. Wang, Q. Sun, X. Wang, T. Wen, J.-J. Yin, P. Wang, R. Bai, X.-Q. Zhang, L.-H. Zhang, A.-H. Lu and C. Chen, *J. Am.Chem.Soc.*, 2015, **137**, 1947-1955.
17. W. Yin, L. Yan, J. Yu, G. Tian, L. Zhou, X. Zheng, X. Zhang, Y. Yong, J. Li, Z. Gu and Y. Zhao, *Acs Nano*, 2014, **8**, 6922-6933.

18. J. Bai, Y. Liu and X. Jiang, *Biomaterials*, 2014, **35**, 5805-5813.
19. G. Song, Q. Wang, Y. Wang, G. Lv, C. Li, R. Zou, Z. Chen, Z. Qin, K. Huo, R. Hu and J. Hu, *Adv. Funct. Mater.*, 2013, **23**, 4281-4292.
20. C. M. Hessel, V. P. Pattani, M. Rasch, M. G. Panthani, B. Koo, J. W. Tunnell and B. A. Korgel, *Nano Letters*, 2011, **11**, 2560-2566.
21. H. Liu, D. Chen, L. Li, T. Liu, L. Tan, X. Wu and F. Tang, *Angew.Chem.Inter.Edi*, 2011, **50**, 891-895.
22. J. Liu, C. Detrembleur, M.-C. De Pauw-Gillet, S. Mornet, C. Jerome and E. Duguet, *Small*, 2015, **11**, 2323-2332.
23. S. Shen, H. Tang, X. Zhang, J. Ren, Z. Pang, D. Wang, H. Gao, Y. Qian, X. Jiang and W. Yang, *Biomaterials*, 2013, **34**, 3150-3158.
24. Z. Zhang, L. Wang, J. Wang, X. Jiang, X. Li, Z. Hu, Y. Ji, X. Wu and C. Chen, *Adv.Mater.*, 2012, **24**, 1418-1423.
25. H. Liu, T. Liu, X. Wu, L. Li, L. Tan, D. Chen and F. Tang, *Adv. Mater.*, 2012, **24**, 755-761.
26. J. L. Vivero-Escoto, I. I. Slowing, C.-W. Wu and V. S. Y. Lin, *J.Am.Chem.Soc.*, 2009, **131**, 3462-+.
27. L. Guo, D. D. Yan, D. Yang, Y. Li, X. Wang, O. Zalewski, B. Yan and W. Lu, *Acs Nano*, 2014, **8**, 5670-5681.
28. Q. Tian, M. Tang, Y. Sun, R. Zou, Z. Chen, M. Zhu, S. Yang, J. Wang, J. Wang and J. Hu, *Adv. Mater.*, 2011, **23**, 3542-3547.
29. M. Zhou, R. Zhang, M. Huang, W. Lu, S. Song, M. P. Melancon, M. Tian, D. Liang and C. Li, *J.Am.Chem.Soc.*, 2010, **132**, 15351-15358.
30. Q. Tian, F. Jiang, R. Zou, Q. Liu, Z. Chen, M. Zhu, S. Yang, J. Wang, J. Wang and J. Hu, *Acs Nano*, 2011, **5**, 9761-9771.
31. Q. Tian, J. Hu, Y. Zhu, R. Zou, Z. Chen, S. Yang, R. Li, Q. Su, Y. Han and X. Liu, *J.Am.Chem.Soc.*, 2013, **135**, 8571-8577.
32. S. Wang, A. Riedinger, H. Li, C. Fu, H. Liu, L. Li, T. Liu, L. Tan, M. J. Barthel, G. Pugliese, F. De Donato, M. S. D'Abbusco, X. Meng, L. Manna, H. Meng and T. Pellegrino, *Acs Nano*, 2015, **9**, 1788-1800.
33. Y. Li, W. Lu, Q. Huang, M. Huang, C. Li and W. Chen, *Nanomedicine*, 2010, **5**, 1161-1171.
34. Y. Huang, Y. Lai, S. Shi, S. Hao, J. Wei and X. Chen, *Chem.-Asian J.*, 2015, **10**, 370-376.
35. A. C. Poulose, S. Veeranarayanan, M. S. Mohamed, Y. Nagaoka, R. R. Aburto, T. Mitcham, P. M. Ajayan, R. R. Bouchard, Y. Sakamoto, Y. Yoshida, T. Maekawa and D. S. Kumar, *Nanoscale*, 2015, **7**, 8378-8388.
36. G. Ku, M. Zhou, S. Song, Q. Huang, J. Hazle and C. Li, *Acs Nano*, 2012, **6**, 7489-7496.
37. X. Liu, W.-C. Law, M. Jeon, X. Wang, M. Liu, C. Kim, P. N. Prasad and M. T. Swihart, *Adv. Healthcare Mater.*, 2013, **2**, 952-957.
38. S. Ramadan, L. Guo, Y. Li, B. Yan and W. Lu, *Small*, 2012, **8**, 3143-3150.
39. M. Zhou, J. Li, S. Liang, A. K. Sood, D. Liang and C. Li, *ACS nano*, 2015, **9**, 7085-7096.
40. X. Liu, Q. Wang, C. Li, R. Zou, B. Li, G. Song, K. Xu, Y. Zheng and J. Hu, *Nanoscale*, 2014, **6**, 4361-4370.
41. B. Li, Q. Wang, R. Zou, X. Liu, K. Xu, W. Li and J. Hu, *Nanoscale*, 2014, **6**, 3274-3282.
42. X. Liu, F. Fu, K. Xu, R. Zou, J. Yang, Q. Wang, Q. Liu, Z. Xiao and J. Hu, *J. Mater. Chem. B*, 2014, **2**, 5358-5367.
43. H. Cabral, Y. Matsumoto, K. Mizuno, Q. Chen, M. Murakami, M. Kimura, Y. Terada, M. R. Kano, K. Miyazono, M. Uesaka, N. Nishiyama and K. Kataoka, *Nat. Nanotech.*, 2011, **6**, 815-823.
44. X. He, X. Bao, H. Cao, Z. Zhang, Q. Yin, W. Gu, L. Chen, H. Yu and Y. Li, *Adv. Funct. Mater.* 2015, **25**, 2831-2839.

45. D. K. Roper, W. Ahn and M. Hoepfner, *J. Phys. Chem. C*, 2007, **111**, 3636-3641.
46. T. Zhou, X. Zhou and D. Xing, *Biomaterials*, 2014, **35**, 4185-4194.
47. H. Chen, T. Moore, B. Qi, D. C. Colvin, E. K. Jelen, D. A. Hitchcock, J. He, O. T. Mefford, J. C. Gore, F. Alexis and J. N. Anker, *Acs Nano*, 2013, **7**, 1178-1187.
48. C. Y. Lai, B. G. Trewyn, D. M. Jeftinija, K. Jeftinija, S. Xu, S. Jeftinija and V. S. Y. Lin, *J. Am.Chem. Soc.*, 2003, **125**, 4451-4459.

Figure Captions

Scheme 1. Schematic illustration of the fabrication of pH and NIR light dual-responsive CuS-Dox drug nanocarries and synergistic antitumor therapeutic effect combining chemotherapy and photothermal ablation of cancer cell in vivo.

Figure 1. (a) TEM image of PAA-CuS NCs. (b) Magnified TEM and HRTEM image (the inset) of PAA-CuS NCs. (c) Hydrodynamic diameter distribution of CuS-Dox. (d) Temperature elevation of the aqueous solution containing CuS NCs with different concentrations under the irradiation of 808 nm with a power density of 2.33 W/cm^2 as a function of irradiation time (0-600 s). (e) Infrared thermal graphic images of water and CuS NCs solution with different concentration (12, 24, 48 μg/mL) under laser irradiation. (f) Plot of temperature change (ΔT) as a function CuS concentration. (g) Temperature elevation of the CuS NCs aqueous solution (96 μg/mL) under irradiation of different power density as a function of time. (h) Photothermal effect of CuS NCs (24 μg/mL) upon being irradiated for 10 min (808 nm) and shutting off the laser. (i) Time constant for heat transfer from the system is determined by applying the linear time data from the cooling period of versus negative natural logarithm (*h*) of driving force temperature.

Figure 2. (a) UV-vis-NIR spectra of free Dox, PAA-CuS NCs and CuS-Dox nanocarries.(Inset: Photographs of CuS, free Dox, and CuS-Dox solution) (b) Fluorescence spectra of CuS-Dox from initial concentration of Dox. (c) Dox release profile of CuS-Dox in different pH values solution at 37 ^{o}C. (d) NIR light-responsive release profile of Dox from CuS-Dox in the pH 5.0 PBS solution under irradiation of different laser power density.

Figure 3. Intracellular fluorescence images of Dox in MCF-7 cells incubated with free Dox (a), CuS-Dox without (b) or with (c) 808 laser irradiation.

Figure 4. In vitro chemo-phothermal combination therapy. Fluorescence images of calcein AM (green, live cells) and propidium iodide (red, dead cells) co-stained MCF-7 cells with (a) different concentration CuS NCs (50, 80, 100 μg/mL) incubation with exposure to the 808 nm laser irradiation, (b) PBS, laser irradiation alone, CuS NCs without laser (100 μg/mL), respectively. The cell viability rate (c) and inhibition rate (d) of MCF-7 cell treated with the free Dox, CuS+Laser, CuS-Dox, and CuS-Dox+Laser, respectively.

Figure 5. Representative photos of the 4T1-tumor-bearing BALB/C mice treated with PBS+Laser, free Dox+Laser, CuS+Laser, CuS-Dox and CuS-Dox+Laser, respectively, at day 1 before treatment and at day 5 and day 9 after treatment.

Figure 6. In vivo chemo-phothermal combination therapy. (a) Tumor volume was measured after treatment administration in different groups (PBS+Laser, free Dox+Laser, CuS+Laser, CuS-Dox and CuS-Dox+Laser, power density = 1.0 W/cm^2, time = 10 min). (b) Weight of mice in different group over time after the treatment. (c) Photographs of tumors from different groups (PBS+Laser, free Dox+Laser, CuS+Laser, CuS-Dox and CuS-Dox+Laser). (d) Histological images of tumors collected from different groups (PBS+Laser, free Dox+Laser, CuS+Laser, CuS-Dox and CuS-Dox+Laser).

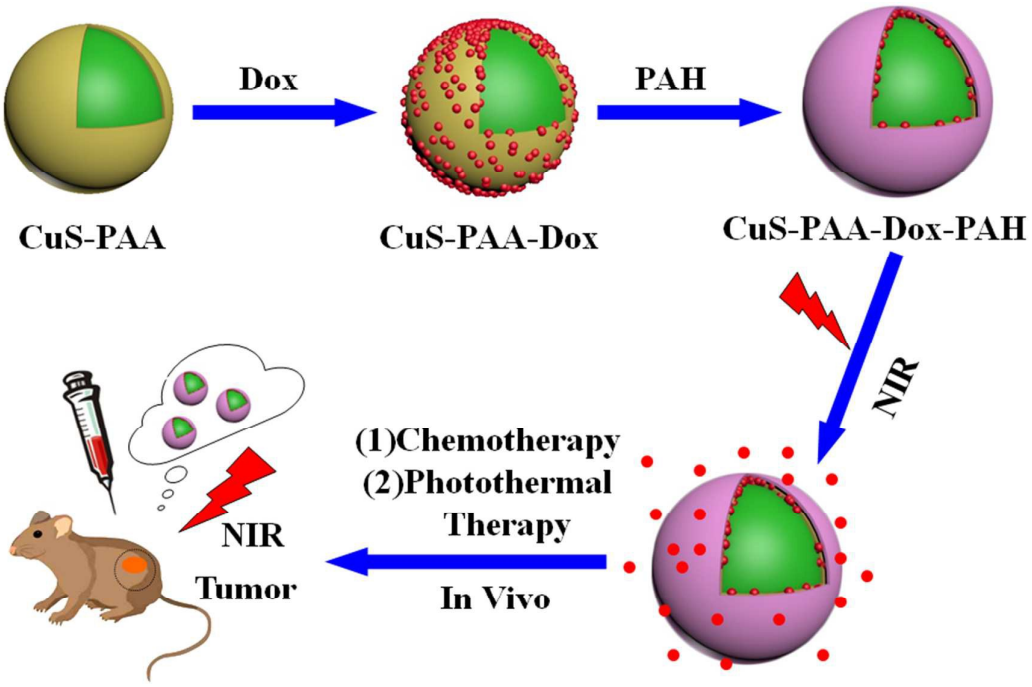

Scheme 1

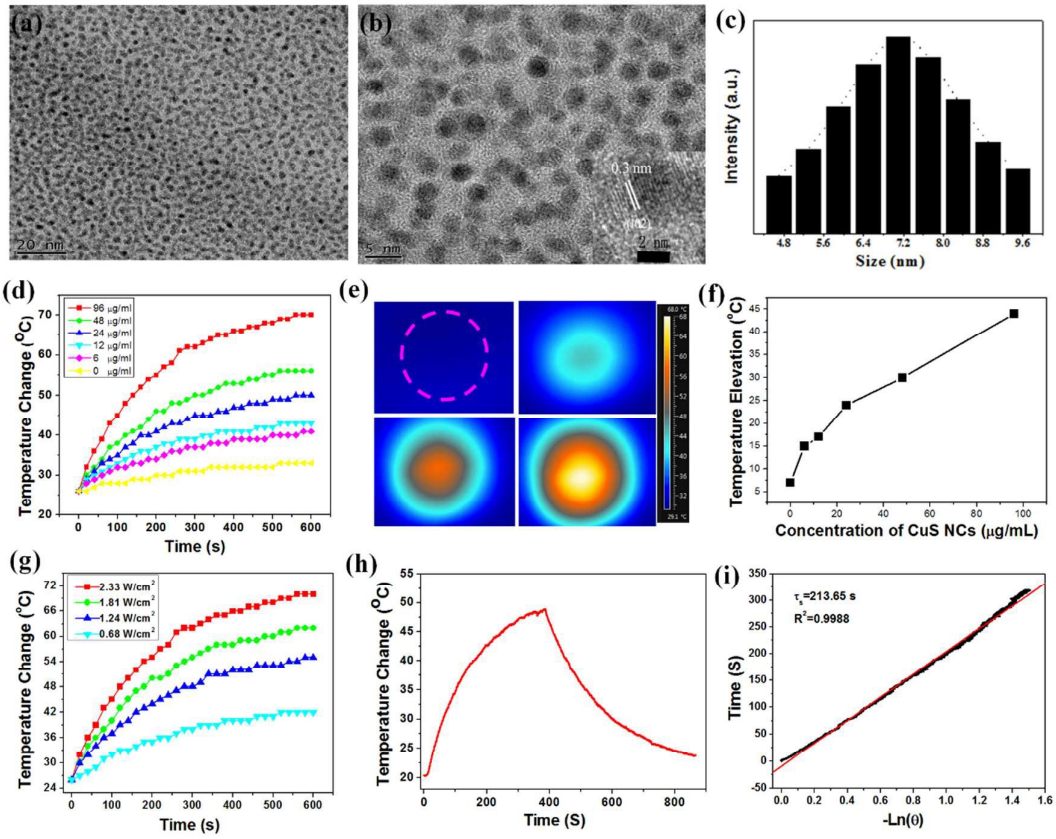

Figure 1

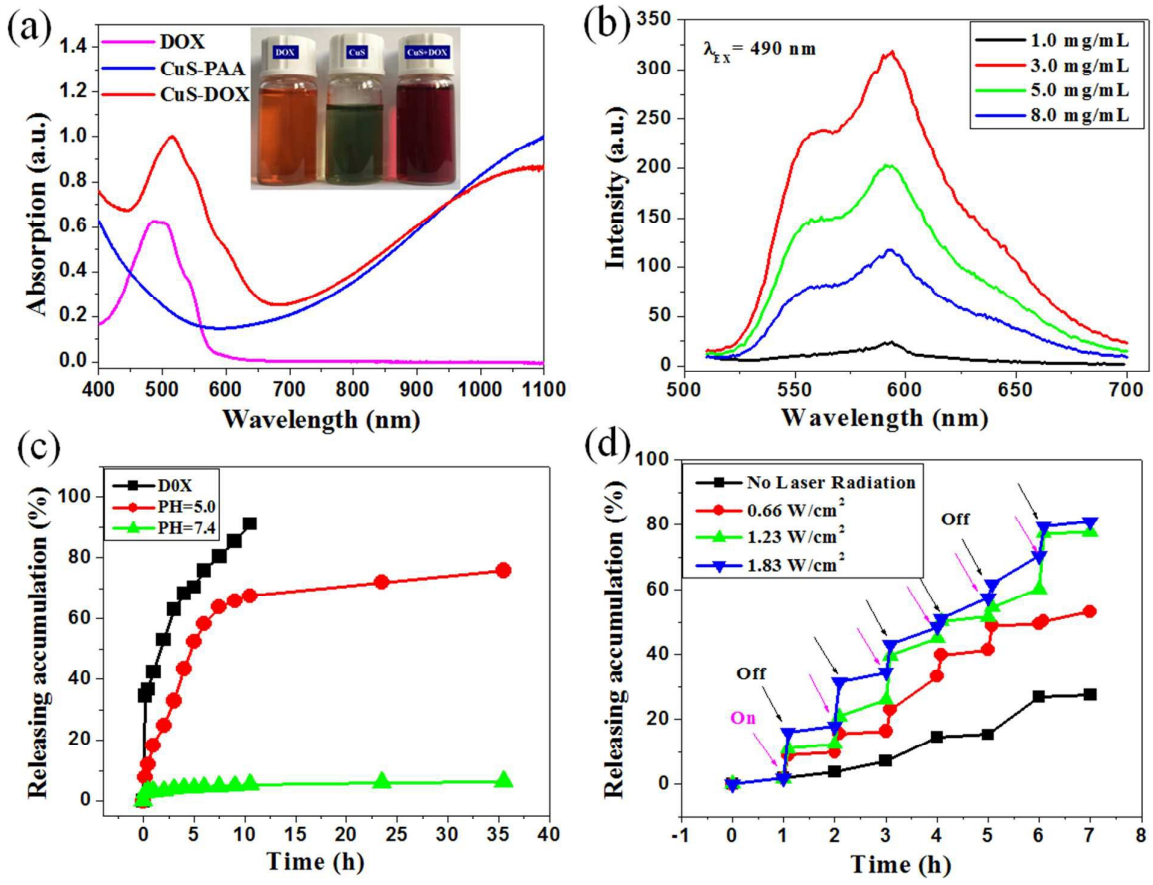

Figure 2

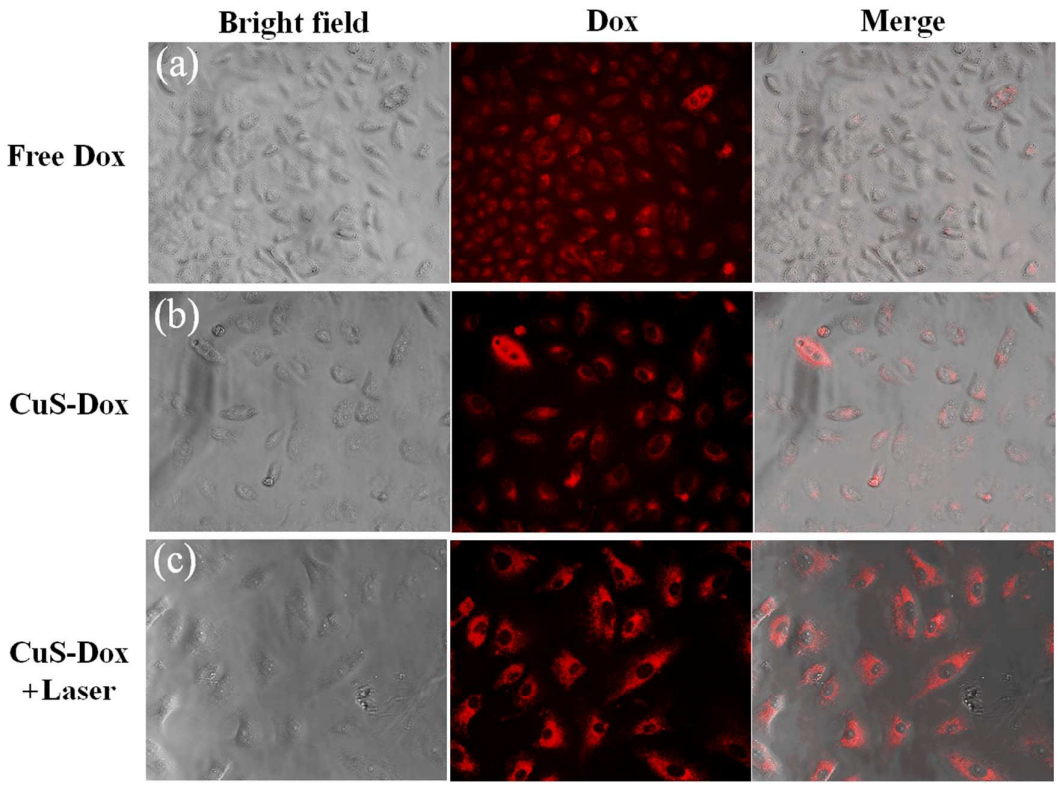

Figure 3

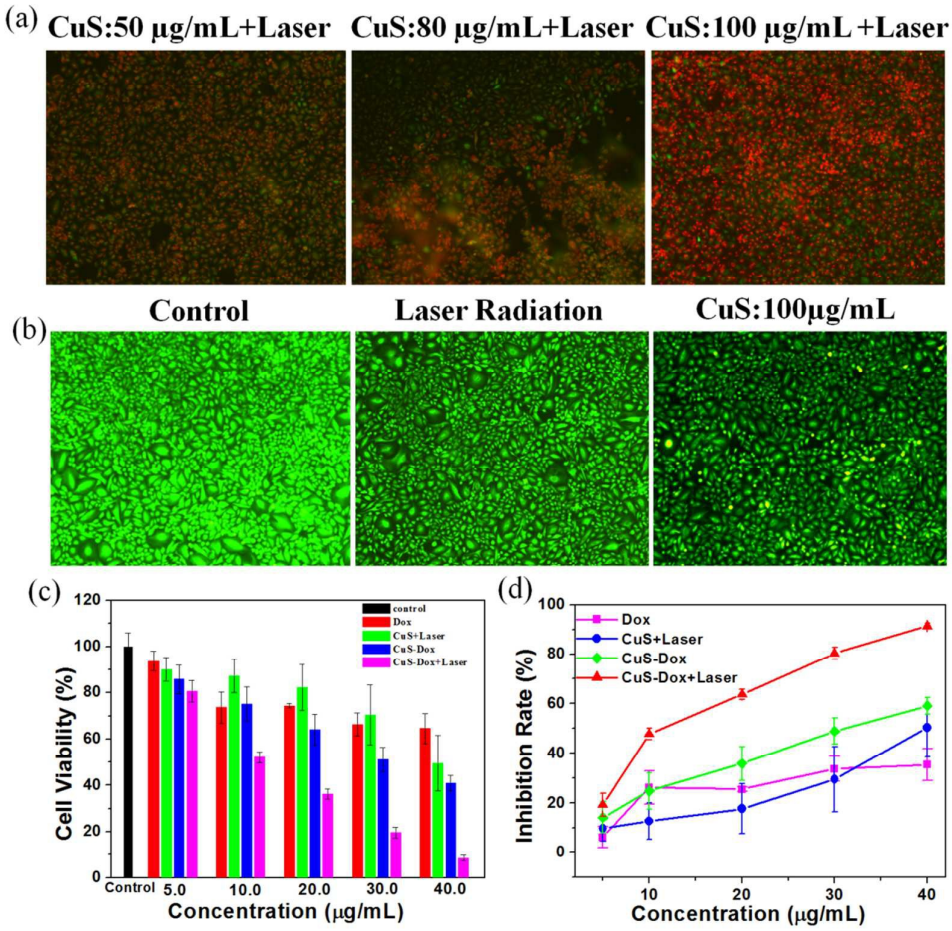

Figure 4

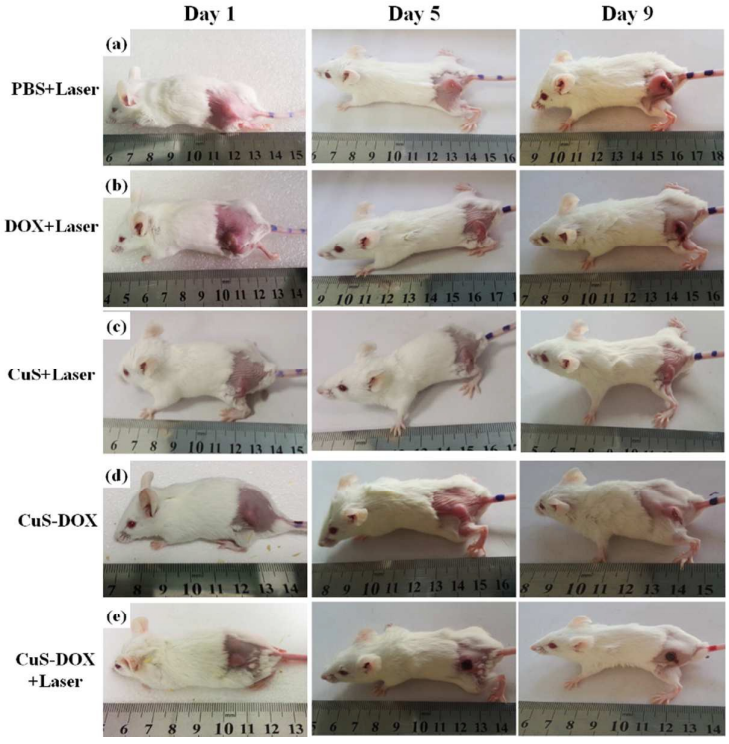

Figure 5

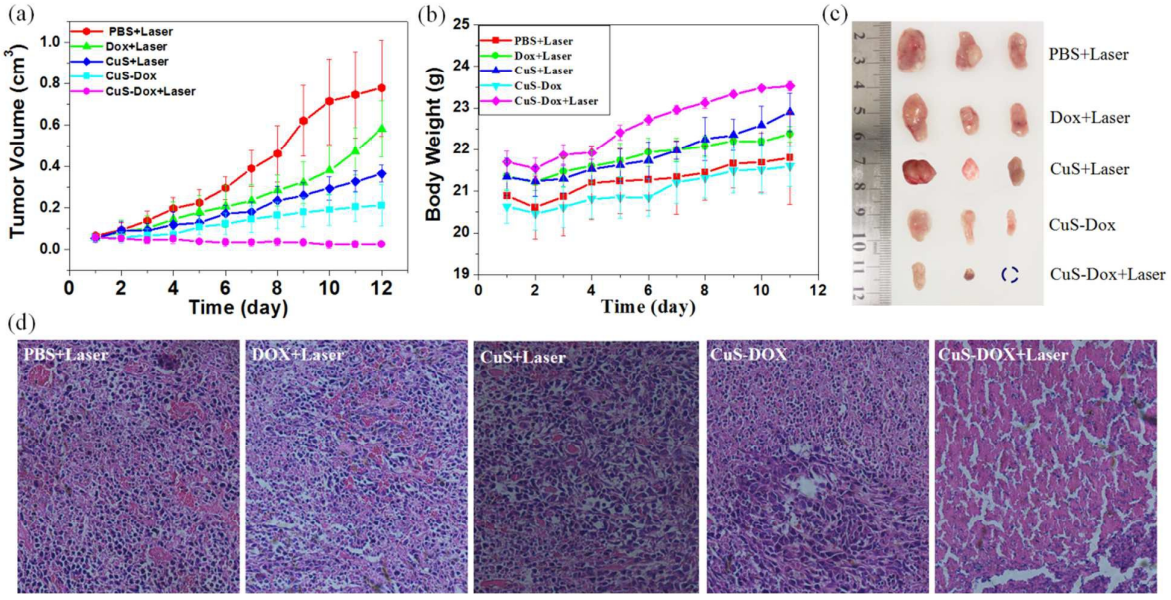

Figure 6